horizontal bar representing the median, and the error bars representing minimum and maximum values.

ACCESSION NUMBERS

RNA-seq data have been submitted to NCBI-GEO under the accession number GSE64867.

SUPPLEMENTAL INFORMATION

Supplemental Information includes Extended Experimental Procedures, six figures, and five movies and can be found with this article online at http://dx.doi.org/10.1016/j.cell.2015.01.043.

ACKNOWLEDGMENTS

We thank B. Reva for helpful consultation regarding TCGA data analyses; S. Karlsson for floxed-*Tgfbr2* mice; F. Costantini for *Rosa-YFP* mice; L. Chin for *TetO-Hras* mice; and L. Polak, J. Levorse, and others for assistance in the mouse facility. We are grateful to extensive interactions and helpful discussions with former and present Fuchs lab members. We appreciate the assistance of RU's Comparative Bioscience Center (an AAALAC facility) for expert care and housing of our mice, the RU Flow Cytometry Resource Center (S. Mazel, Director) and Weill Cornell Medical College Genomics Resources Core Facility for Illumina sequencing (J. Xiang, Director). N.O was supported by Human Frontier Science Program and the Japan Society for the Promotion of Science and is now supported by NIH K99-R00 pathway to independence award. E.F. is an investigator of the Howard Hughes Medical Institute. This work was supported by grants from the NIH and from the New York State Department of Health (NYSTEM-C029559) to E.F. and from the National Cancer Institute (K99-CA178197) to N.O.

Received: September 26, 2014
Revised: December 21, 2014
Accepted: January 13, 2015
Published: February 26, 2015

REFERENCES

Beck, B., Driessens, G., Goossens, S., Youssef, K.K., Kuchnio, A., Caauwe, A., Sotiropoulou, P.A., Loges, S., Lapouge, G., Candi, A., et al. (2011). A vascular niche and a VEGF-Nrp1 loop regulate the initiation and stemness of skin tumours. Nature *478*, 399–403.

Berns, A. (2005). Stem cells for lung cancer? Cell *121*, 811–813.

Beronja, S., Livshits, G., Williams, S., and Fuchs, E. (2010). Rapid functional dissection of genetic networks via tissue-specific transduction and RNAi in mouse embryos. Nat. Med. *16*, 821–827.

Bigarella, C.L., Liang, R., and Ghaffari, S. (2014). Stem cells and the impact of ROS signaling. Development *141*, 4206–4218.

Boumahdi, S., Driessens, G., Lapouge, G., Rorive, S., Nassar, D., Le Mercier, M., Delatte, B., Caauwe, A., Lenglez, S., Nkusi, E., et al. (2014). SOX2 controls tumour initiation and cancer stem-cell functions in squamous-cell carcinoma. Nature *511*, 246–250.

Bruna, A., Darken, R.S., Rojo, F., Ocaña, A., Peñuelas, S., Arias, A., Paris, R., Tortosa, A., Mora, J., Baselga, J., and Seoane, J. (2007). High TGFβ-Smad activity confers poor prognosis in glioma patients and promotes cell proliferation depending on the methylation of the PDGF-B gene. Cancer Cell *11*, 147–160.

Chen, C.R., Kang, Y., Siegel, P.M., and Massagué, J. (2002). E2F4/5 and p107 as Smad cofactors linking the TGFβ receptor to c-myc repression. Cell *110*, 19–32.

Chen, W., Sun, Z., Wang, X.-J., Jiang, T., Huang, Z., Fang, D., and Zhang, D.D. (2009). Direct interaction between Nrf2 and p21(Cip1/WAF1) upregulates the Nrf2-mediated antioxidant response. Mol. Cell *34*, 663–673.

Chin, L., Tam, A., Pomerantz, J., Wong, M., Holash, J., Bardeesy, N., Shen, Q., O'Hagan, R., Pantginis, J., Zhou, H., et al. (1999). Essential role for oncogenic Ras in tumour maintenance. Nature *400*, 468–472.

Cui, W., Fowlis, D.J., Bryson, S., Duffie, E., Ireland, H., Balmain, A., and Akhurst, R.J. (1996). TGFβ1 inhibits the formation of benign skin tumors, but enhances progression to invasive spindle carcinomas in transgenic mice. Cell *86*, 531–542.

Derynck, R., and Miyazono, K. (2008). The TGF-β family (Woodbury, New York: Cold Spring Harbor Laboratory Press).

Diehn, M., Cho, R.W., Lobo, N.A., Kalisky, T., Dorie, M.J., Kulp, A.N., Qian, D., Lam, J.S., Ailles, L.E., Wong, M., et al. (2009). Association of reactive oxygen species levels and radioresistance in cancer stem cells. Nature *458*, 780–783.

Gomis, R.R., Alarcón, C., Nadal, C., Van Poznak, C., and Massagué, J. (2006). C/EBPβ at the core of the TGFβ cytostatic response and its evasion in metastatic breast cancer cells. Cancer Cell *10*, 203–214.

Gorrini, C., Harris, I.S., and Mak, T.W. (2013). Modulation of oxidative stress as an anticancer strategy. Nat. Rev. Drug Discov. *12*, 931–947.

Greaves, M., and Maley, C.C. (2012). Clonal evolution in cancer. Nature *481*, 306–313.

Grivennikov, S.I., Greten, F.R., and Karin, M. (2010). Immunity, inflammation, and cancer. Cell *140*, 883–899.

Grotendorst, G.R., Smale, G., and Pencev, D. (1989). Production of transforming growth factor β by human peripheral blood monocytes and neutrophils. J. Cell. Physiol. *140*, 396–402.

Guasch, G., Schober, M., Pasolli, H.A., Conn, E.B., Polak, L., and Fuchs, E. (2007). Loss of TGFβ signaling destabilizes homeostasis and promotes squamous cell carcinomas in stratified epithelia. Cancer Cell *12*, 313–327.

Hanahan, D., and Weinberg, R.A. (2011). Hallmarks of cancer: the next generation. Cell *144*, 646–674.

Hope, K.J., Jin, L., and Dick, J.E. (2004). Acute myeloid leukemia originates from a hierarchy of leukemic stem cell classes that differ in self-renewal capacity. Nat. Immunol. *5*, 738–743.

Ijichi, H., Chytil, A., Gorska, A.E., Aakre, M.E., Fujitani, Y., Fujitani, S., Wright, C.V.E., and Moses, H.L. (2006). Aggressive pancreatic ductal adenocarcinoma in mice caused by pancreas-specific blockade of transforming growth factor-β signaling in cooperation with active Kras expression. Genes Dev. *20*, 3147–3160.

Kelland, L. (2007). The resurgence of platinum-based cancer chemotherapy. Nat. Rev. Cancer *7*, 573–584.

Koinuma, D., Tsutsumi, S., Kamimura, N., Taniguchi, H., Miyazawa, K., Sunamura, M., Imamura, T., Miyazono, K., and Aburatani, H. (2009). Chromatin immunoprecipitation on microarray analysis of Smad2/3 binding sites reveals roles of ETS1 and TFAP2A in transforming growth factor β signaling. Mol. Cell. Biol. *29*, 172–186.

Kreso, A., and Dick, J.E. (2014). Evolution of the cancer stem cell model. Cell Stem Cell *14*, 275–291.

Lapouge, G., Beck, B., Nassar, D., Dubois, C., Dekoninck, S., and Blanpain, C. (2012). Skin squamous cell carcinoma propagating cells increase with tumour progression and invasiveness. EMBO J. *31*, 4563–4575.

Lu, S.-L., Herrington, H., Reh, D., Weber, S., Bornstein, S., Wang, D., Li, A.G., Tang, C.-F., Siddiqui, Y., Nord, J., et al. (2006). Loss of transforming growth factor-β type II receptor promotes metastatic head-and-neck squamous cell carcinoma. Genes Dev. *20*, 1331–1342.

Lushchak, V.I. (2012). Glutathione homeostasis and functions: potential targets for medical interventions. J. Amino Acids *2012*, 736837.

Malanchi, I., Peinado, H., Kassen, D., Hussenet, T., Metzger, D., Chambon, P., Huber, M., Hohl, D., Cano, A., Birchmeier, W., and Huelsken, J. (2008). Cutaneous cancer stem cell maintenance is dependent on β-catenin signalling. Nature *452*, 650–653.

Massagué, J. (2012). TGFβ signalling in context. Nat. Rev. Mol. Cell Biol. *13*, 616–630.

Massagué, J., Seoane, J., and Wotton, D. (2005). Smad transcription factors. Genes Dev. *19*, 2783–2810.

Meacham, C.E., and Morrison, S.J. (2013). Tumour heterogeneity and cancer cell plasticity. Nature *501*, 328–337.

Mullen, A.C., Orlando, D.A., Newman, J.J., Lovén, J., Kumar, R.M., Bilodeau, S., Reddy, J., Guenther, M.G., DeKoter, R.P., and Young, R.A. (2011). Master transcription factors determine cell-type-specific responses to TGF-β signaling. Cell *147*, 565–576.

Muñoz, N.M., Upton, M., Rojas, A., Washington, M.K., Lin, L., Chytil, A., Sozmen, E.G., Madison, B.B., Pozzi, A., Moon, R.T., et al. (2006). Transforming growth factor β receptor type II inactivation induces the malignant transformation of intestinal neoplasms initiated by Apc mutation. Cancer Res. *66*, 9837–9844.

Nischt, R., Roop, D.R., Mehrel, T., Yuspa, S.H., Rentrop, M., Winter, H., and Schweizer, J. (1988). Aberrant expression during two-stage mouse skin carcinogenesis of a type I 47-kDa keratin, K13, normally associated with terminal differentiation of internal stratified epithelia. Mol. Carcinog. *1*, 96–108.

Notta, F., Doulatov, S., Laurenti, E., Poeppl, A., Jurisica, I., and Dick, J.E. (2011). Isolation of single human hematopoietic stem cells capable of long-term multilineage engraftment. Science *333*, 218–221.

Oshimori, N., and Fuchs, E. (2012a). The harmonies played by TGF-β in stem cell biology. Cell Stem Cell *11*, 751–764.

Oshimori, N., and Fuchs, E. (2012b). Paracrine TGF-β signaling counterbalances BMP-mediated repression in hair follicle stem cell activation. Cell Stem Cell *10*, 63–75.

Schober, M., and Fuchs, E. (2011). Tumor-initiating stem cells of squamous cell carcinomas and their control by TGF-β and integrin/focal adhesion kinase (FAK) signaling. Proc. Natl. Acad. Sci. USA *108*, 10544–10549.

Seoane, J., Le, H.-V., Shen, L., Anderson, S.A., and Massagué, J. (2004). Integration of Smad and forkhead pathways in the control of neuroepithelial and glioblastoma cell proliferation. Cell *117*, 211–223.

Siegle, J.M., Basin, A., Sastre-Perona, A., Yonekubo, Y., Brown, J., Sennett, R., Rendl, M., Tsirigos, A., Carucci, J.A., and Schober, M. (2014). SOX2 is a cancer-specific regulator of tumour initiating potential in cutaneous squamous cell carcinoma. Nat. Commun. *5*, 4511.

Thuault, S., Valcourt, U., Petersen, M., Manfioletti, G., Heldin, C.-H., and Moustakas, A. (2006). Transforming growth factor-β employs HMGA2 to elicit epithelial-mesenchymal transition. J. Cell Biol. *174*, 175–183.

Visvader, J.E., and Stingl, J. (2014). Mammary stem cells and the differentiation hierarchy: current status and perspectives. Genes Dev. *28*, 1143–1158.

Yamashiro, Y., Takei, K., Umikawa, M., Asato, T., Oshiro, M., Uechi, Y., Ishikawa, T., Taira, K., Uezato, H., and Kariya, K. (2010). Ectopic coexpression of keratin 8 and 18 promotes invasion of transformed keratinocytes and is induced in patients with cutaneous squamous cell carcinoma. Biochem. Biophys. Res. Commun. *399*, 365–372.

EXTENDED EXPERIMENTAL PROCEDURES

Mouse Strains

We used *Tgfbr2* floxed (Levéen et al., 2002), *Rosa26-lox-STOP-lox-EYFP* (*Rosa-YFP*) (Srinivas et al., 2001), *TetO-Hras* (*TRE-Hras1*^{G12V}) (Chin et al., 1999) and *K14-CreER* (Vasioukhin et al., 1999) mice. *Nude* mice were from Charles River Laboratories.

Lentiviral Constructs

To generate the TGF-β reporter LV, we subcloned DNA fragments of 12X-repeated Smad-binding elements (SBE, 5′-AGCCAGACA-3′) (Dennler et al., 1998), a minimal CMV promoter (mCMV), and a P2A-based (Szymczak-Workman et al., 2012) bicistronic construct NLS-mCherry-P2A-CreER into pLKO-MCS vector (Beronja et al., 2010). We further inserted PGK-iRFP (Filonov et al., 2011) for in vitro experiments, and PGK-rtTA3 for in vivo experiments, and an shRNA hairpin DNA for KD. For K14-CreER genetic background, we used the TGF-β reporter LV lacking CreER. For the NRF2 reporter, we subcloned DNA fragments of 6X-repeated antioxidant-response elements (ARE, 5′-TCACAGTGACTCAGCAAAATT-3′) followed by mCMV and NLS-mCherry. For *Hras*^{G12V} transduction in vitro, we used MSCV-Hras^{G12V}-IRES-Hyg retroviral vector.

In Vitro Virus Transduction

For lenti- or retro-viral infections in culture, cells were plated in 6-well plate at 1.0×10^5 cells per well and incubated with viruses in the presence of polybrene (20 μg/ml) for 30 min, and then plates were spun at 1,100 *g* for 30 min at 37°C (lenti) or 32°C (retro) in a Thermo IEC CL40R centrifuge. Infected cells were purified by FACS on the basis of iRFP expression or alternatively selected with puromycin or hygromycin.

Immunofluorescence and Imaging

For immunofluorescence microscopy of tumor sections, dissected tumors were fixed with 4% PFA in PBS for 15 min at room temperature, washed with PBS, and embedded in OCT (Tissue Tek). Cryosections were cut at a thickness of 10 μm on a Leica cryostat and mounted on SuperFrost Plus slides (VWR) and permeabilized for 10 min in 0.3% Triton X-100 in PBS. For immunolabeling and visualization of in vitro culture cells, cells were seeded onto coverslips and fixed with 4% paraformaldehyde (PFA) in PBS for 10 min at room temperature. When immunolabeling with mouse antibodies, sections were incubated with the M.O.M. blocking kit according to manufacturer's instructions (Vector Laboratories). For pSMAD2 immunolabeling, reagents and protocols from TSA Plus kit were used (PerkinElmer). For immunolabeling to detect BrdU and Cisplatin-DNA adducts, tissue sections were pretreated with 1N HCl for 1 h at 37°C before adding the antibodies (anti-BrdU, 1:100, Alexa 488-conjugated mouse mAb, Life Technologies); (anti-cisplatin-DNA adduct, 1:250, Millipore). The following primary antibodies were used: pSMAD2 (rabbit, 1:1,000, Cell Signaling), integrin α6 (rat, 1:2,000, BD), RFP/mCherry (rabbit, 1:3,000, MBL International), mCherry (goat, 1:3,000, Acris), anti-GFP/YFP (chicken, 1:2,000, Abcam), TGF-β (rabbit, 1:100, R&D systems), CD44 (rat, 1:250, BioLegend), K10 (rabbit, 1:1,000, Covance), NRF2 (rabbit, 1:500, MBL International), p21 (rabbit, 1:1,000, Santa Cruz), γ-H2AX (rabbit, 1:500, Cell Signaling), cleaved caspase-3 (rabbit, 1:500, Cell Signaling), GSTα (goat, 1:500, Abcam), CD140a (rat, 1:50, BioLegend), CD31 (rat, 1:50, BioLegend), CD11b (rat, 1:100, BioLegend), CD64 (mouse, 1:50, BioLegend), Ly6c (rat, 1:50, BioLegend), CD3 (rat, 1:100, BioLegend), Endoglin (goat, 1:250, Abcam), E-cadherin (rabbit, 1:500, Cell Signaling), ZEB2/SIP1 (rabbit, 1:250, Abcam), K5 (guinea pig, 1:1,000, Fuchs lab), K13 (rabbit, 1:500, Abcam), K18 (rabbit, 1:500, Fuchs lab), α-tubulin (mouse, 1:1,000, Sigma). Sections treated with primary antibodies were incubated at 4°C for overnight. After washing with PBS with 0.1% Triton X-100 (PBST), sections were treated for 30 min at room temperature with secondary antibodies conjugated with Alexa 488, 546, or 647 (Life Technologies). Slides were washed, counterstained with 4'6'-diamidino-2-phenilindole (DAPI) and mounted in Prolong Gold (Life Technologies). Imaging was performed on Zeiss Axio Observer Z1 equipped with ApoTome.2 or Axioplan 2 using ×10/0.45 air or ×20/0.8 air. Images were collected using Zeiss ZEN software. For thick tumor sections (200–300 μm), sections were permeabilized for >1 hr and incubated with primary antibodies for 24 hr at room temperature, followed by 5–6 hr of washing in PBST, exchanging every 1 hr. Sections were then incubated with secondary antibodies for 24 hr at room temperature, followed by 5–6 hr of washing in PBST, exchanging every 1 hr. Then, we cleared tumor sections by following a tissue-clearing method (Ertürk et al., 2012) and collected images with a PerkinElmer Volocity spinning disk system.

Immunoblotting

Total cell lysates were prepared using RIPA (20 mM Tris-HCl (pH 8.0), 150 mM NaCl, 1 mM EDTA, 1 mM EGTA, 1% Triton X-100, 0.5% deoxycorate, 0.1% SDS) or IP lysis buffer (25 mM Tris-HCl [pH 7.4], 150 mM NaCl, 1 mM EDTA, 1% NP-40, 5% glycerol for immunoprecipitation) supplemented with protease inhibitors (Complete mini, Roche) and 25 mM β-glycerophosphate, 10 mM NaF, 1 mM Na3VO4, or using directly NuPAGE LDS sample buffer (Life Technologies). The protein concentrations of clarified supernatants were measured by using BCA Protein Assay Kit (Thermo Scientific). The rabbit anti-p21 antibodies (5 μg, Santa Cruz) coupled to Dynabeads Protein G (Life Technologies) for 1 hr at 4°C was incubated with cell lysates (500 μg) for 2 hr at 4°C. The immunoprecipitates were washed with IP lysis buffer, eluted by the elution buffer before adding SDS sample buffer. Gel electrophoresis was performed using 4%–12% NuPAGE Bis-Tris gradient gels (Life Technologies), transferred to PVDF membranes (Immobilon-P^{SQ}, Millipore). Membranes were blocked for 1 hr in Odyssey blocking buffer (LI-COR), then incubated with primary antibodies in the blocking buffer supplemented with 0.1% Tween 20 overnight at 4°C. After washing with PBS with 0.1% Tween 20 (PBSTw),

membranes were incubated with secondary antibodies in the blocking buffer with 0.1% Tween 20 and 0.01% SDS. Membranes were washed in PBSTw, then in PBS before imaging on an Odyssey infrared scanner (LI-COR). Primary antibodies used were: pSMAD2 (rabbit, 1:3,000, Cell Signaling), SMAD2/3 (mouse, 1:2,000, BD), Nrf2 (rabbit, 1:3,000, MBL International), p21 (rabbit, 1:2,000, Santa Cruz), mCherry (goat, 1:3,000, Acris), Hras (rabbit, 1:1,000, Santa Cruz), phospho-ERK1/2 (rabbit, 1:1,000, Cell Signaling), α-tubulin (mouse, 1:3,000, Sigma). Secondary antibodies were conjugated to IRDye680 or IRDye800 (1:15,000, LI-COR).

FACS

Tumors were dissected from mice, minced by scalpels in chilled dish on ice, and treated with 0.25% collagenase (Sigma) in HBSS (Gibco) for overnight at 4°C. The cell suspension was pipet up and down 20 times and pelleted at 300 × *g* for 10 min at 4°C. Precipitated cells were resuspended in 0.25% trypsin (Gibco) to dissociate further at 37°C for 15 min, and filtered through a 70- and 40-μm strainers. Cells were pelleted at 300 × g for 10 min at 4°C and then resuspended in wash buffer (PBS with 5% FBS) and incubated with surface antibodies for FACS. The following surface antibodies were used: CD49f/integrin α6-PerCP-Cy5.5 (1:250, BD), CD44-PE-Cy7 (1:100, BioLegend), CD34-FITC (1:100, eBioscience), CD45-APC (1:500, BioLegend), CD11b-APC (1:200, BioLegend), CD31-APC (1:100, BioLegend), CD140a-APC (1:100, BioLegend). DAPI was used to exclude dead cells. Cell isolations were performed on FACSAria cell sorters equipped with FACSDiva software (BD). Sorted cells were used for RNA preparation for RNA-seq, qRT-PCR, colony formation assay and transplantation onto *Nude* mice. For measuring ROS levels in tumor cells, single cell suspension were incubated in cell culture media containing CellROX Green Reagent according to manufacture's instructions (Life Technologies).

RNA Purification, RNA-Seq, and qRT-PCR

Total RNA from FACS-purified cells directly sorted into TRI Reagent (Sigma) was purified using Direct-zol RNA MiniPrep Kit (Zymo Research) per manufacturer's instructions. Quality of the RNA for sequencing was determined using an Agilent 2100 Bioanalyzer; all samples used had RNA integrity numbers >9. Library preparation using the Illumina TrueSeq mRNA sample preparation kit was performed at the Weill Cornell Medical College Genomic Core facility (New York), and RNAs were paired-end sequenced on Illumina HiSeq 2000 machines. Alignment of reads was done using Tophat with the mm9 build of the mouse genome. Transcript assembly and differential expression was determined using Cufflinks with Refseq mRNAs to guide assembly (Trapnell et al., 2010). Analysis of RNA-seq data was done using the cummeRbund package in R (Trapnell et al., 2012). Transcripts regulated both greater than and less than 2-fold were used in GO term and KEGG pathway analysis to find enriched functional annotations. For real-time qRT-PCR, equivalent amounts of RNA were reverse-transcribed by SuperScript VILO cDNA Synthesis Kit (Life Technologies). cDNAs were normalized to equal amounts using primers against *Ppib2*. cDNAs were mixed with indicated primers and SYBR green PCR Master Mix (Sigma), and qRT-PCR was performed on an Applied Biosystems 7900HT Fast Real-Time PCR system. The following primer sequences were used (5′ →3′):

Ppib2 forward: GTGAGCGCTTCCCAGATGAGA, *Ppib2* reverse: TGCCGGAGTCGACAATGATG,
mCherry forward: CTTCGCCTGGGACATCCTGT, *mCherry* reverse: TCTTGACCTCGGCGTCGTAGT,
Gsta1 forward: CATTGAAGTGGTGAAGCACG, *Gsta1* reverse: CTGGACTGTGAGCTGAGTGG,
Gsta2 forward: TTGAAGTAGTGAAGCACGGG, *Gsta2* reverse: ATTGGGAGCTGAGTGGAGAA,
Gsta3 forward: GATAGGCTCCATTCTTCCCC, *Gsta3* reverse: TCCGGCTTTTTAACAAGAAAA,
Gsta4 forward: TGATTGCCGTGGCTCCATTTA, *Gsta4* reverse: CAACGAGAAAAGCCTCTCCGT,
Gsta5 forward: CACGGGGCAGTATGGAGTCC, *Gsta5* reverse: AAGGCAGGGAAGTAGCGATTTTT,
Me1 forward: TCAACAAGGACTTGGCTTTTACT, *Me1* reverse: TGCAGGTCCATTAACAGGAGAT,
Gpx2 forward: GCCTCAAGTATGTCCGACCTG, *Gpx2* reverse: GGAGAACGGGTCATCATAAGGG,
Hmox1 forward: AAGCCGAGAATGCTGAGTTCA, *Hmox1* reverse: GCCGTGTAGATATGGTACAAGGA,
Slc7a11 forward: GGCACCGTCATCGGATCAG, *Slc7a11* reverse: CTCCACAGGCAGACCAGAAAA,
Nqo1 forward: AGGATGGGAGGTACTCGAATC, *Nqo1* reverse: AGGCGTCCTTCCTTATATGCTA,
Nfe2l2 forward: TCTTGGAGTAAGTCGAGAAGTGT, *Nfe2l2* reverse: GTTGAAACTGAGCGAAAAAGGC,
Maff forward: GCGTGTTCTCGCTCAACTC, *Maff* reverse: CGACAAGCACGCACTGAG,
Keap1 forward: TGCCCCTGTGGTCAAAGTG, *Keap1* reverse: GGTTCGGTTACCGTCCTGC,
Cdkn1a forward: ATCCCGACTCTTGACATTGC, *Cdkn1a* reverse: ACCCTAGACCCACAATGCAG,
Serpine1 forward: CCTACCCCACAAAGGTCTCA, *Serpine1* reverse: GGCCACCATTTGATCTGTCT,
Tgfbi forward: GGGCTGCACCATATTGAGAT, *Tgfbi* reverse: AGATGCCGTAGTTCCCCTTT.

shRNA Sequences for Gene Knockdown

For knockdown experiments, we used clones from the Broad Institute's Mission TRC mouse library. We tested the knockdown efficiency of 8–10 independent shRNAs for each gene and used the following clones and target sequence:

The scramble shRNA (Sigma SHC002, CAACAAGATGAAGAGCACCAA), *Cdkn1a* #4 (TRCN0000042587, GATTGGTCTTCTGCAA GAGAA), *Cdkn1a* #8 (TRCN0000042584, GACCAGCCTGACAGATTTCTA), *Nfe2l2* #7 (TRCN0000054659, CTTGAAGTCTTCAG CATGTTA), *Nfe2l2* #10 (TRCN0000054662, GCCTTACTCTCCCAGTGAATA), *Maff* #7 (TRCN0000219025, GACTCTTCCACACTCT TATTT), *Maff* #8 (TRCN0000225793, TTGCACGAATCTAAGTTATTC), *Keap1* #2 (TRCN0000099446, GCCCAATTCATGGCTCA

CAAA), *Keap1* #6 (TRCN, 0000295016, GTGCATCGACTGGGTCAAATA). These sequences were cloned from the library vectors into LV TGF-β reporter or pLKO-H2B-mRFP vector.

SUPPLEMENTAL REFERENCES

Dennler, S., Itoh, S., Vivien, D., ten Dijke, P., Huet, S., and Gauthier, J.M. (1998). Direct binding of Smad3 and Smad4 to critical TGF β-inducible elements in the promoter of human plasminogen activator inhibitor-type 1 gene. EMBO J. *17*, 3091–3100.

Ertürk, A., Becker, K., Jährling, N., Mauch, C.P., Hojer, C.D., Egen, J.G., Hellal, F., Bradke, F., Sheng, M., and Dodt, H.U. (2012). Three-dimensional imaging of solvent-cleared organs using 3DISCO. Nat. Protoc. *7*, 1983–1995.

Filonov, G.S., Piatkevich, K.D., Ting, L.M., Zhang, J., Kim, K., and Verkhusha, V.V. (2011). Bright and stable near-infrared fluorescent protein for in vivo imaging. Nat. Biotechnol. *29*, 757–761.

Levéen, P., Larsson, J., Ehinger, M., Cilio, C.M., Sundler, M., Sjöstrand, L.J., Holmdahl, R., and Karlsson, S. (2002). Induced disruption of the transforming growth factor β type II receptor gene in mice causes a lethal inflammatory disorder that is transplantable. Blood *100*, 560–568.

Srinivas, S., Watanabe, T., Lin, C.S., William, C.M., Tanabe, Y., Jessell, T.M., and Costantini, F. (2001). Cre reporter strains produced by targeted insertion of EYFP and ECFP into the ROSA26 locus. BMC Dev. Biol. *1*, 4.

Szymczak-Workman, A.L., Vignali, K.M., and Vignali, D.A.A. (2012). Design and construction of 2A peptide-linked multicistronic vectors. Cold Spring Harb Protoc *2012*, 199–204.

Trapnell, C., Williams, B.A., Pertea, G., Mortazavi, A., Kwan, G., van Baren, M.J., Salzberg, S.L., Wold, B.J., and Pachter, L. (2010). Transcript assembly and quantification by RNA-Seq reveals unannotated transcripts and isoform switching during cell differentiation. Nat. Biotechnol. *28*, 511–515.

Trapnell, C., Roberts, A., Goff, L., Pertea, G., Kim, D., Kelley, D.R., Pimentel, H., Salzberg, S.L., Rinn, J.L., and Pachter, L. (2012). Differential gene and transcript expression analysis of RNA-seq experiments with TopHat and Cufflinks. Nat. Protoc. *7*, 562–578.

Vasioukhin, V., Degenstein, L., Wise, B., and Fuchs, E. (1999). The magical touch: genome targeting in epidermal stem cells induced by tamoxifen application to mouse skin. Proc. Natl. Acad. Sci. USA *96*, 8551–8556.

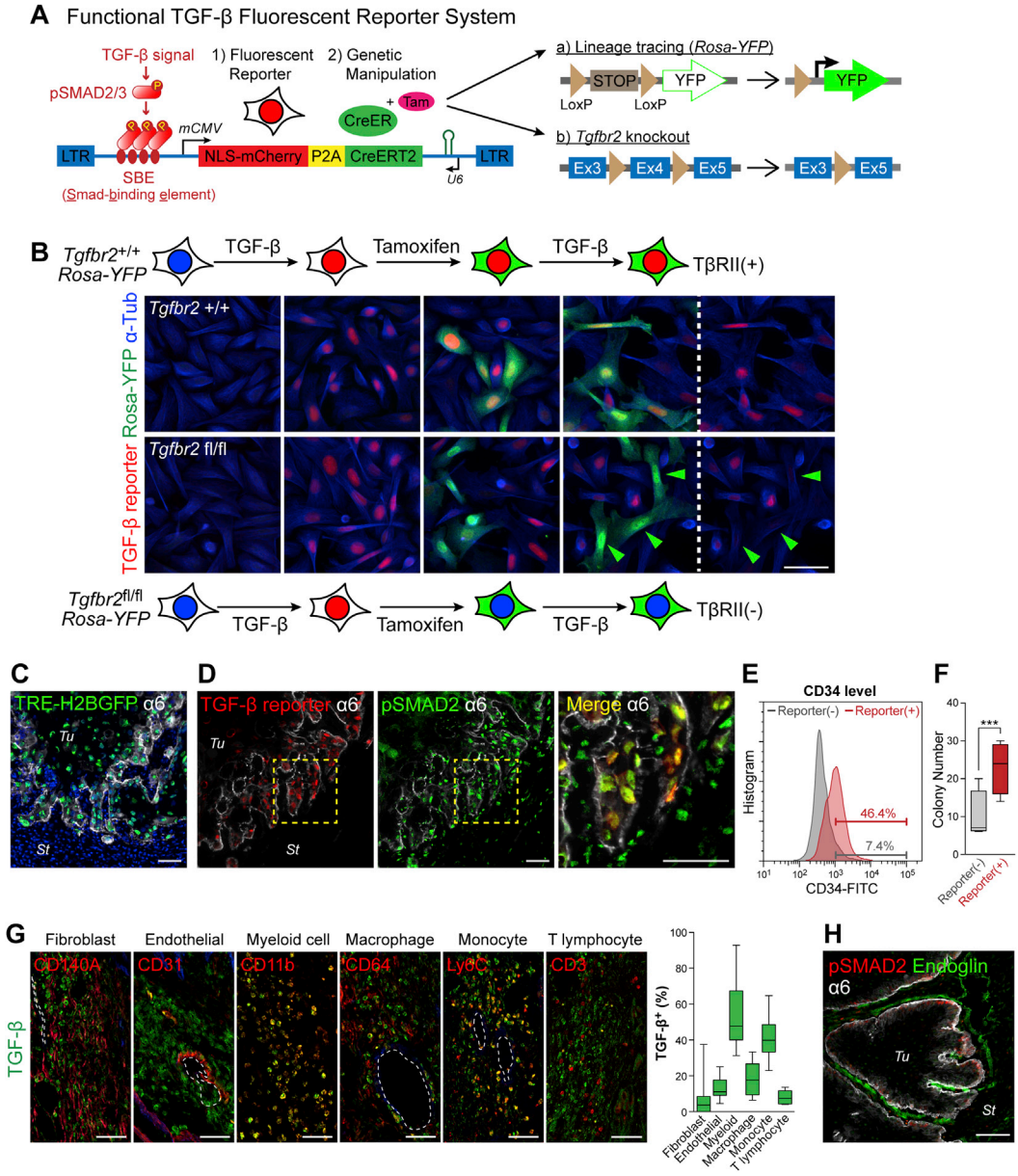

Figure S1. In Vitro Test of a New TGF-β Reporter System, and TGF-β Ligand and Signaling in Tumors In Vivo, Related to Figure 1

(A) Experimental scheme of a TGF-β reporter system and genetic manipulations by TGF-β reporter CreER-Tamoxifen (Tam).

(B) Mouse keratinocytes (*Tgfbr2*$^{+/+}$ and *Tgfbr2*$^{fl/fl}$) were transduced with lentiviral TGF-β reporter construct. TGF-β treatment followed by tamoxifen (4-hydroxytamoxifen) administration resulted in TβRII^{+} cells and TβRII^{neg} from *Tgfbr2*$^{+/+}$ and *Tgfbr2*$^{fl/fl}$, respectively. In *Tgfbr2*$^{fl/fl}$ background, CreER activation induced YFP expression and TβRII-deficiency.

(C) Immunofluorescence image of *TRE-Hras*^{G12V}*; TRE-H2BGFP* tumor induced by lentiviral transduction of a TGF-β reporter construct containing rtTA3.

(D) Coimmunostaining of TGF-β reporter (NLS-mCherry) and pSMAD2. Yellow dotted box showed colocalization of TGF-β reporter and pSMAD2 in the tumor epithelia, but not in the stroma.

(E) Flow cytometry analysis of CD34 expression in integrin α6^{Hi}CD44^{+} tumor basal cells based on TGF-β reporter activity. (F) FACS-isolated tumor basal cells were plated and allowed to grow for 2 weeks in media. Quantification of colony numbers is shown.

(G) Coimmunostaining of TGF-β ligands and a marker of fibroblasts (CD140a), endothelial cells (CD31), myeloid cells (CD11b), macrophages (CD64), monocytes (Ly6c) and T lymphocytes (CD3). Dotted lines or circles indicate the lumen of blood vessels.

(H) Immunostaining of pSMAD2 and an endothelial marker, endoglin.

Data are box-and-whisker plots (F and G). Scale bars, 50 μm.

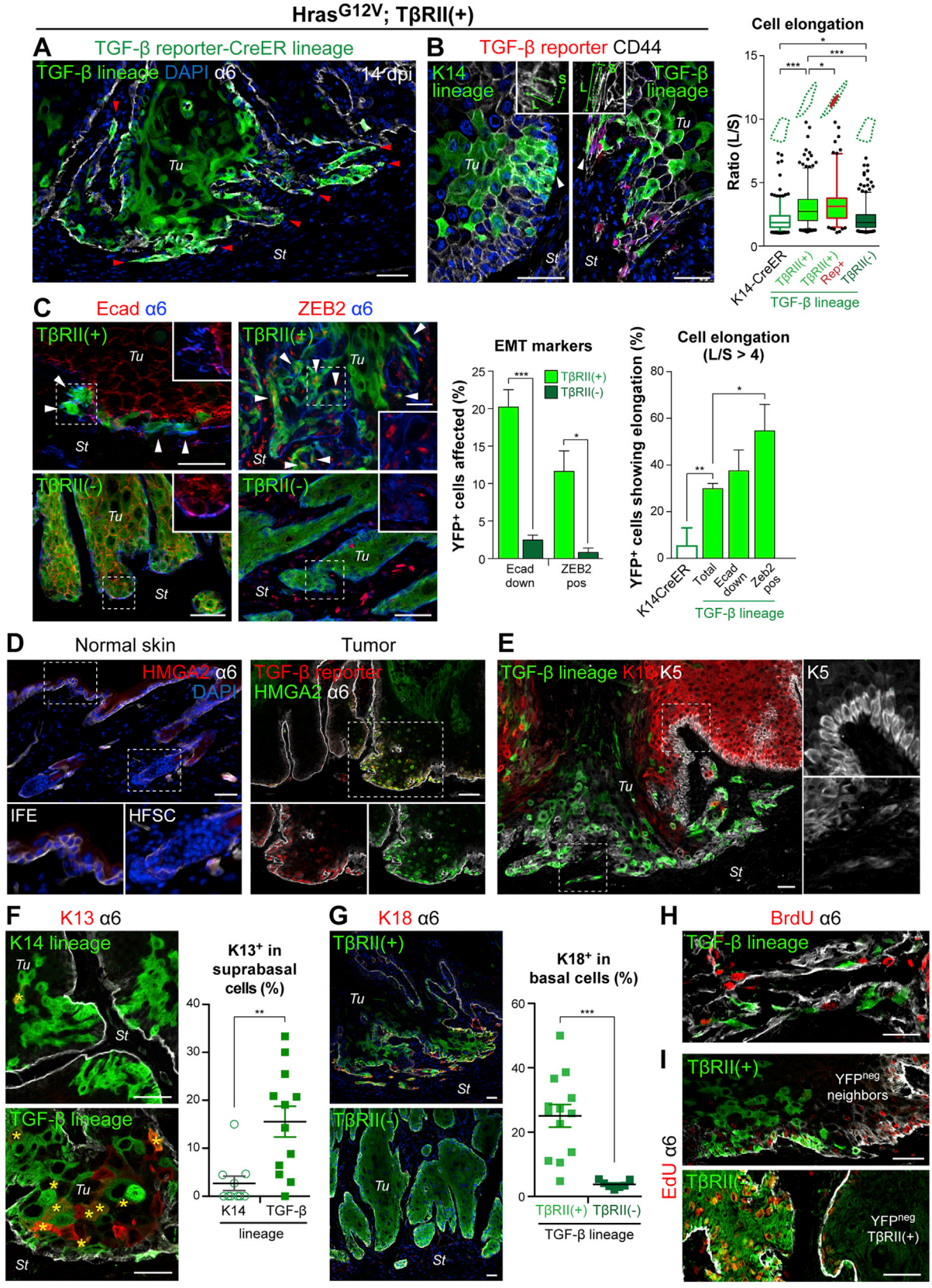

(legend on next page)

Figure S2. EMT and Differentiation Markers in TGF-β Reporter$^+$ Progenies, Related to Figure 2

(A) Representative image of the distribution of TGF-β reporter-CreER (TGFβ-CreER)-induced YFP$^+$ cellular lineage at 14 dpi. Note that invasive tips in tumor substructures were occupied by YFP$^+$ cells (red arrowheads).

(B) Comparison of cellular morphologies between K14-CreER and TGFβ-CreER-driven YFP$^+$ clones. (Insets) Surface marker CD44 (white) was used to outline tumor cells for measurements of long-to-short axis (L/S) ratios. (Right) Quantification of L/S ratio of YFP$^+$ tumor basal cells (n=148–329 cells) in K14-CreER- and Tβ-CreER-induced TβRII$^+$ and TβRII^{neg} lineages. Data are box-and-whisker plots.

(C) Immunofluorescence of EMT markers. Ecad expression was downregulated in TβRII$^+$YFP$^+$ cells, whereas TβRII^{neg}YFP$^+$ cells were maintained Ecad expression at the tumor-stroma interface. EMT transcription factor ZEB2 was detected in some TβRII$^+$YFP$^+$ cells, but not in TβRII^{neg} cells, while stromal cells expressed similar levels of ZEB2 in both tumors. (Right) Quantifications of YFP$^+$ cells affected in EMT markers and its cell elongation.

(D) During normal homeostasis, the self-renewal factor HMGA2 is not appreciably expressed in interfollicular epidermis (IFE) or hair follicle stem cells (HFSC). In SCC tumors, however, HMGA2 is highly upregulated, where it significantly overlaps with TGF-β reporter activity.

(E) Expression of epidermal basal marker, Keratin 5 (K5), and suprabasal marker, Keratin 10 (K10), in TGFβ-CreER marked TβRII$^+$ tumor cells and their progenies. (Inset) K5 staining in different regions of the tumor basal layer. Note that YFP$^+$ cells showed lower levels of K5 expression, and barely expressed K10 in the suprabasal layers.

(F) An aberrant SCC differentiation marker, Keratin 13 (K13), was largely confined to suprabasal layers of TGFβ-CreER-derived lineage clones. (Right) Quantification of the overlaps between K13 and YFP$^+$ suprabasal cells of K14 lineage or TGF-β lineage (n=10 and 13 clones).

(G) Keratin 18 (K18) staining with TβRII$^+$ or TβRII^{neg} YFP$^+$ cell clones. (Right) Quantification of the overlaps between K18 and YFP$^+$ basal cells in TβRII$^+$ or TβRII^{neg} cell clones (n= 13 and 7 clones).

(H) Representative image of BrdU labeling (4 hr) in tumors with TβRII$^+$YFP$^+$ cells (2 d after Tam injection). Note that YFP$^+$ cells incorporate BrdU less frequently compared to YFP^{neg} neighboring cells.

(I) Representative images of EdU labeling (12 hr) in tumors with TβRII$^+$ or TβRII^{neg} YFP$^+$ cells (7 days after Tam injection). Note that (Top) TβRII$^+$YFP$^+$ cells incorporated EdU less frequently compared to surrounding neighbors, whereas (Bottom) TβRII^{neg}YFP$^+$ cells incorporated EdU more frequently than surrounding TβRII$^+$YFP^{neg} cells.

Quantification data are in Figure 2C. Data are mean ± SEM (C, F and G). Scale bars, 50 μm.

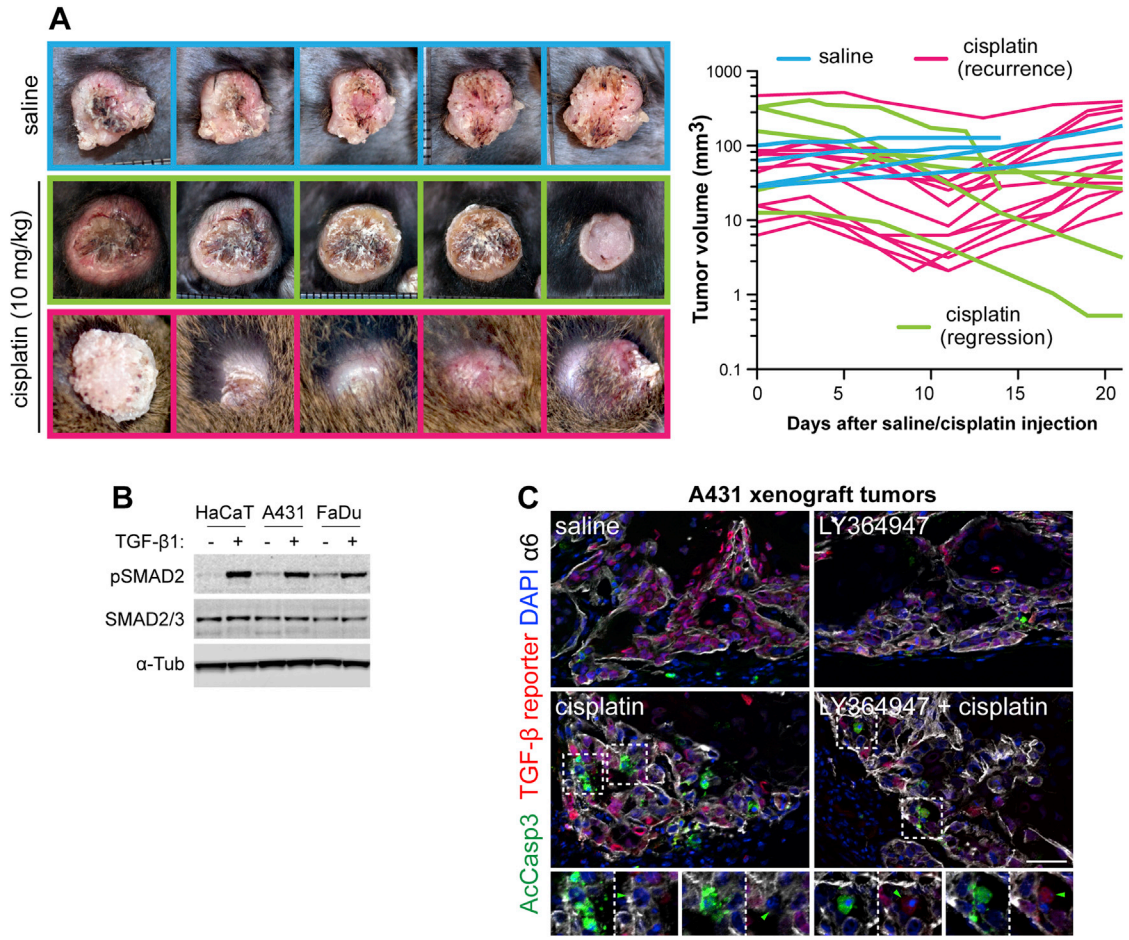

Figure S3. Cisplatin-Induced Tumor Regression and Recurrence, and Human SCC Xenotransplantation, Related to Figure 4

(A) Representative time-course images of tumor growth, regression, and recurrence on mice treated with cisplatin or saline (control). The graph shows the tumor volume after treatments.

(B) Immunoblots of lysates from human keratinocytes (HaCaT) and SCC (A431 and FaDu) cell lines. Note that all cell lines showed increase in pSMAD2 level after TGF-β stimulation.

(C) Immunofluorescence of tumor sections of TGF-β reporter-transduced A431 transplanted tumors treated with a specific TβRI inhibitor, LY364947, and/or cisplatin. Note that LY364947 treatment diminished TGF-β reporter activity in the tumors (dim) and reduced resistance to cisplatin-induced apoptosis ($AcCaps3^{+}$).

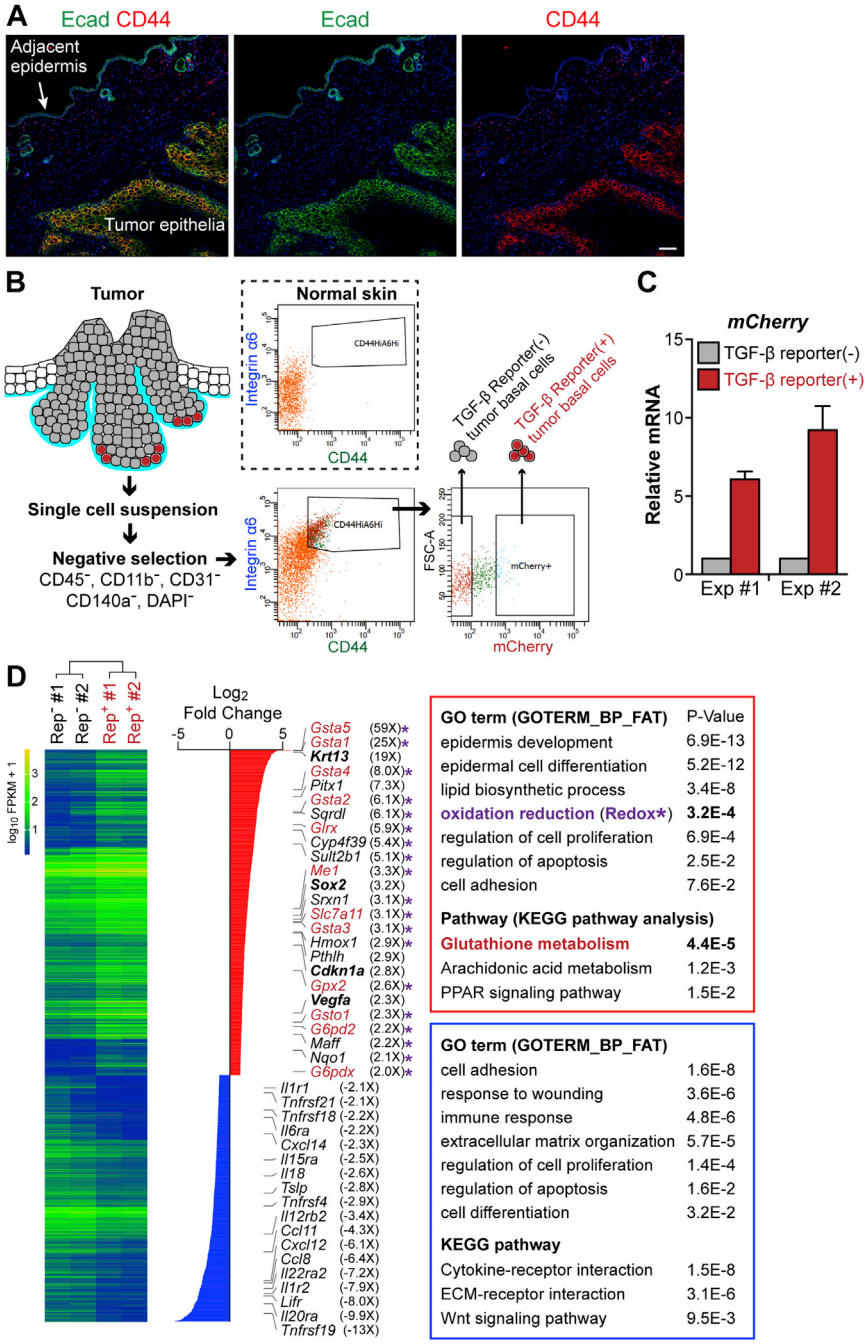

Figure S4. Isolation of TGF-β Reporter$^+$ Cells from Primary Tumors In Vivo and a Summary of RNA-seq Analysis, Related to Figure 5

(A) Immunofluorescence of E-cadherin (Ecad) and CD44 in section with tumor epithelia and adjacent epidermis. Note that CD44 expression was specific to tumor epithelia while Ecad was detected in both.

(B) Scheme of fluorescence-activated cell sorting (FACS) strategy to isolate tumor basal cells with or without TGF-β reporter activity. From the lineage-negative population, total and mCherry$^+$ SCC-SCs were 8.1% ± 1.8% and 0.5% ± 0.1%, respectively (n=8, SEM). (Dotted box) Normal skin samples were used as a negative control for $\alpha6^{Hi}CD44^+$ cell population.

(C) qRT-PCR of mCherry mRNA in two independent FACS-isolated tumor basal cell populations with or without TGF-β reporter activity. Data are mean ± SEM.

(D) A summary of differentially expressed up- and downregulated genes, and GO term and pathway analyses. Scale bars, 50 μm.

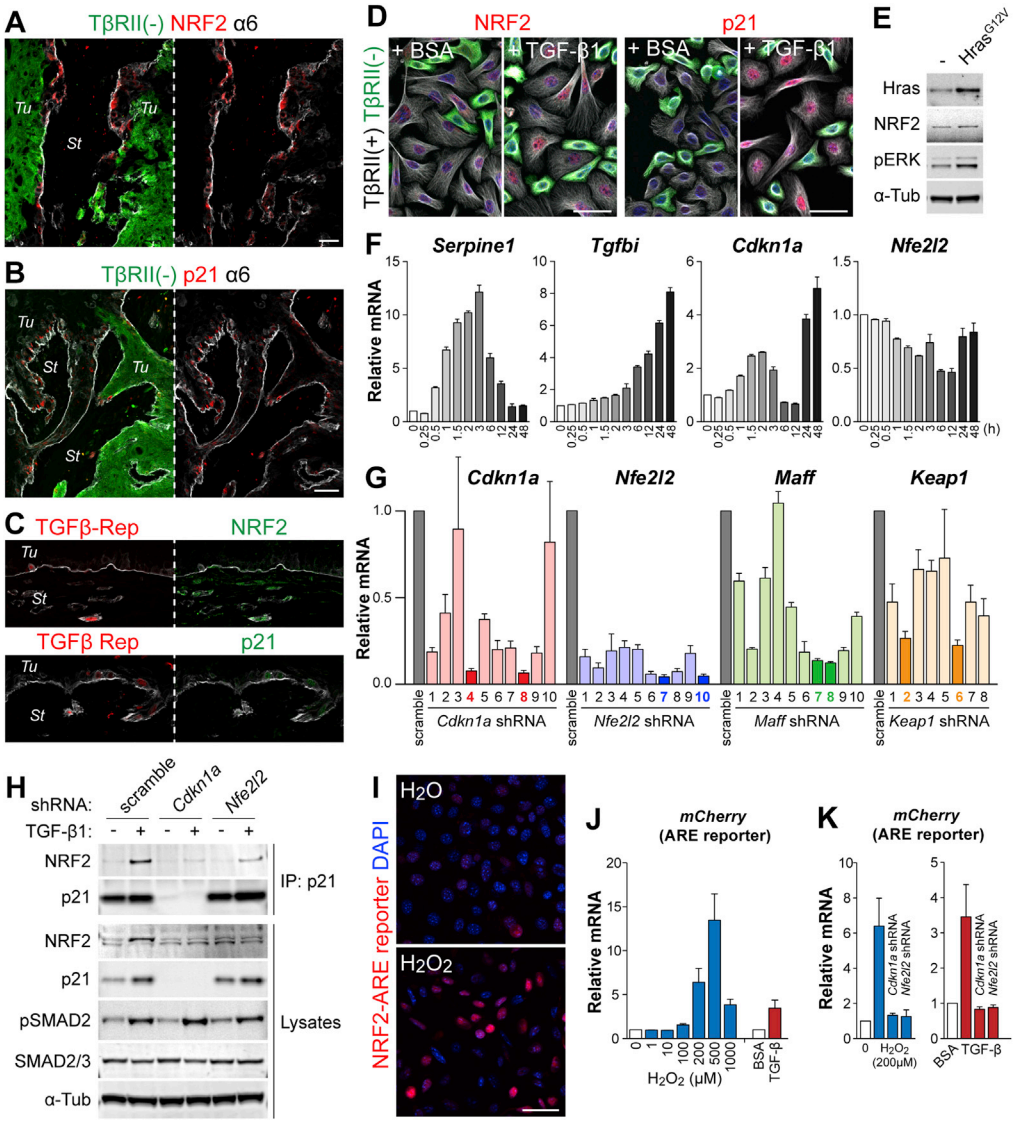

Figure S5. p21, NRF2 and NRF2-ARE Reporter, Related to Figure 6

(A and B) Immunofluorescence of (A) NRF2 and (B) p21 in tumors with TβRII^{neg} clones (shown in green). Note that high levels of expression of both proteins were detected in a subset of neighboring TβRII^{+} tumor cells.

(C) Immunofluorescence of TGF-β reporter and NRF2 or p21 in papillomas.

(D) TβRII^{+} YFP^{neg} and TβRII^{neg}YFP^{+} cells were established as in Figure 3A and cocultured on coverslips. TGF-β treatment induced p21 and NRF2 expression (nuclear accumulation) in predominantly in TβRII^{+}YFP^{neg} MKs.

(E) Immunoblotting of lysates from HRas^{G12V}-transformed and untransformed mouse keratinocytes (MKs).

(F) qRT-PCR analysis using mRNA from HRas^{G12V}-transformed MKs stimulated with TGF-β for different durations. Primers for *Serpine1* and *Tgfbi* were used as positive controls.

(G) shRNA tests for knocking down *Cdkn1a*, *Nfe2l2*, *Maff*, and *Keap1* genes. Knockdown efficiency was normalized with the expression level in control scramble shRNA-transduced cells.

(H) Coimmunoprecipitation of endogenous p21 and NRF2 in TGF-β-treated Hras^{G12V}-transformed 1° MKs transduced with scramble control, *Cdkn1a*, or *Nfe2l2* shRNA. Complexes (IP) and whole cell lysates were analyzed by immunoblotting with indicated antibodies.

(I) In vitro tests of the NRF2-ARE fluorescent reporter. MKs transduced with a lentiviral NRF2-ARE reporter were treated with hydrogen peroxide (100 μM H_2O_2) or H_2O control for 24 hr.

(J) qRT-PCR analysis of *mCherry* mRNA (ARE reporter) in MKs treated with different concentrations of H_2O_2 (1–1,000 μM, 8 hr) and TGF-β (100 pM, 36 hr).

(K) qRT-PCR analysis of *mCherry* mRNA in *Cdkn1a* or *Nfe2l2* shRNA-transduced MKs treated with H_2O_2 (200 μM, 8 hr) or TGF-β (100 pM, 36 hr). Data are mean ± SEM (E–G, J and K). Scale bars, 50 μm.

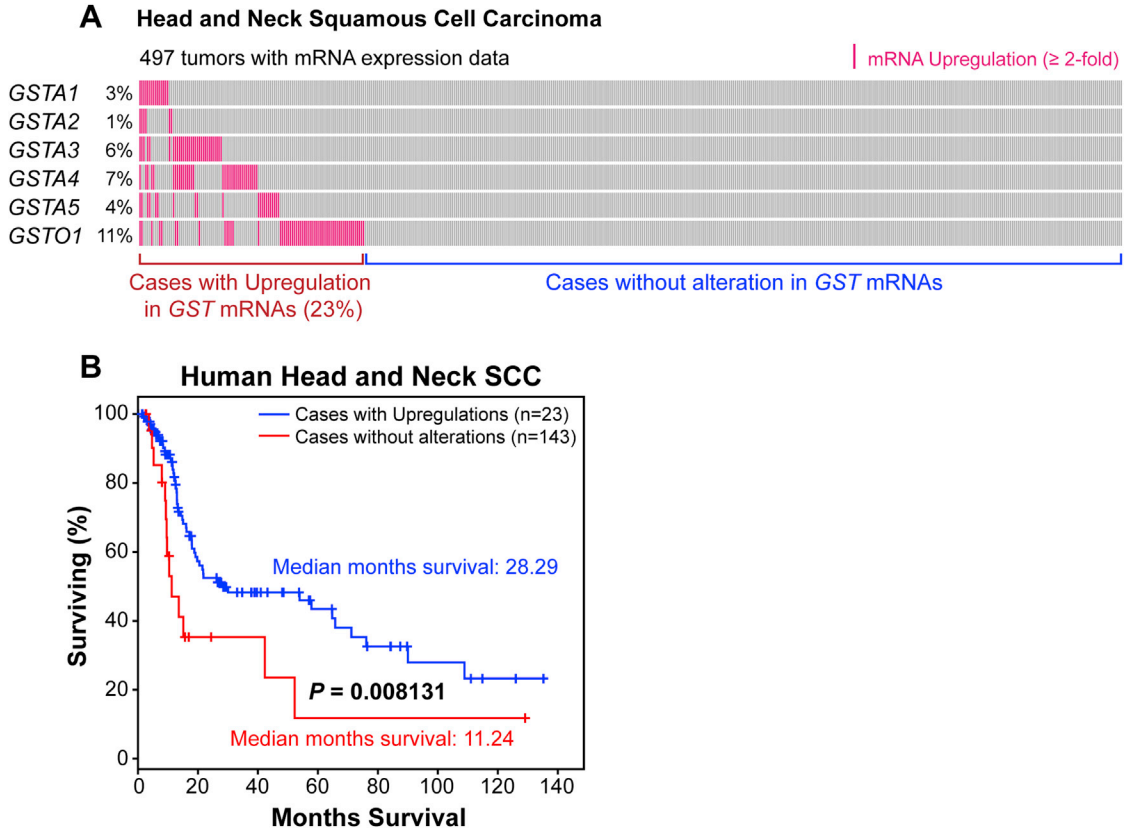

Figure S6. Human TCGA Data Analysis of GST Genes Affected by TGF-β, Related to Figure 7

(A) Summary of 497 TCGA human head and neck SCCs with mRNA expression data. Red vertical bars show cases with ≥ 2-fold mRNA upregulation in indicated GST genes.

(B) Kaplan-Meier survival curves based on the cases in (A). Note that cases with upregulation show poor survival compared to ones without alterations.